Effects of Upstream Wake Phasing on Transonic Axial Compressor Performance

S. P. R. Nolan
e-mail: sprn@alum.mit.edu

B. B. Botros

C. S. Tan

J. J. Adamczyk

E. M. Greitzer

Department of Aeronautics and Astronautics,
Gas Turbine Laboratory,
MIT,
Cambridge, MA 02139

S. E. Gorrell
Department of Mechanical Engineering,
Brigham Young University,
Provo, UT 84602
e-mail: sgorrell@byu.edu

The effect on rotor work of the phase of an upstream wake relative to the rotor is examined computationally and analytically for a transonic blade row. There can be an important impact on the time-mean performance when the time-dependent circulation of the shed vortices in the wake is phase-locked to the rotor position, as it occurs when there is strong interaction between the rotor static pressure field and the upstream vanes. The rotor work is found to depend on the path of the wake vortices as they travel through the blade passage; for the configurations examined, the calculated change in time-mean rotor work was approximately 3%. It is shown that the effect on work input can be analyzed in terms of the influence of the time-mean relative stagnation pressure nonuniformity associated with the unsteady (but phase-locked) wake vortex flow field, in that the changes in vortex path alter the location of the nonuniformity relative to the rotor. Lower pressure rise and work input occurs when the rotor blade is embedded in a region of low time-mean relative stagnation pressure than when immersed in a region of high relative stagnation pressure. In addition to the work changes, which are essentially two-dimensional effects, it is demonstrated that the location of the wake may affect the tip clearance flow, implying a potential impact on the pressure rise capability and rotor stability limits. Model calculations are presented to give estimates of the magnitude and nature of this phenomenon. [DOI: 10.1115/1.4000572]

1 Introduction

The design of highly loaded, high Mach number (HLHM) compressors (i.e., compressors with supersonic relative Mach numbers in an embedded stage) presents challenges specific to the operating regime, because the aerodynamic coupling between blade rows is enhanced by both the loading and the high Mach number. In this paper, one aspect of this coupling is examined: the interaction between the pressure field of a downstream rotor blade row and the shedding of wake vortices from an upstream inlet guide vane (IGV) row. In this situation, there can be a definite phase relative to the rotor, at which the wake vortices from the vane row enter, and convect through the rotor. In other words, for a given rotor geometry and inlet Mach number, the wake shedding can be phase-locked to the rotor position so that the wake vortices travel on the same path for each rotor passage. It is shown there can be appreciable differences in the rotor work as this path is changed by changes in the inlet guide vane-rotor axial spacing. While these effects are present in a subsonic compressor, they are much less important because of the greatly reduced upstream influence of the rotor pressure field.

Some aspects of the interactions between blade rows in an HLHM compressor have been described previously by Gorrell et al. [1,2]. The geometry used, which is the Air Force Research Laboratory (AFRL) stage matching investigation (SMI) compressor, had inlet guide vanes that were straight with a thick trailing edge. The vanes were designed to produce a wake representative of the wake produced by a high pressure ratio, low aspect ratio fan stage. In one set of investigations, a combination of the inlet guide vane plus a rotor was examined experimentally and computationally at three different guide vane-rotor axial spacings, referred to below as spacings A, B, and C, with magnitudes of 29%, 58%, and 124% of the rotor pitch at midspan. Decreases of 0.6 points in efficiency and 1.6% in work input were found as the spacing was reduced from C to A.

The trend seen in the SMI experiments and computations is contrary to that observed in low speed experiments [3–5], where both efficiency and compressor work increased as axial spacing between blade rows was decreased. Smith [6] explained that this increase is due to enhanced energy added to the wake compared with the freestream fluid during passage through the rotor, which reduces the mixing losses (see Refs. [7–10] for discussion of this effect).

This paper presents a mechanism for alterations in the rotor performance that is important at high rotor Mach numbers and which thus addresses, at least in part, the different behaviors seen at low and high Mach numbers. As a first step in illustrating the mechanism, Fig. 1 shows a midspan snapshot from an unsteady three-dimensional computation[1] of the vorticity field downstream of the inlet guide vane for the A and C blade row spacings. Regions of high vorticity, which roll up into vortices, are shed from the inlet guide vane as the rotor bow shock sweeps past. The vortex cores are larger and more intense for spacing A than for spacing C. Furthermore, the vorticity nonuniformity for spacing A is not mixed out even at the exit of the rotor.

Gorrell et al. [2] described a simple model of the vortex shedding in this configuration, which suggests that the strength of the vortices is approximately proportional to vane thickness. A variation in the vane circulation (variation in the velocity difference across the vane) is created as the shock passes, due to the difference in axial locations at which the shock intersects the upper and lower surfaces. A time-varying vane circulation, in turn, means that vorticity must be shed from the trailing edge. As time increases, the shock moves upstream of the vane passage and the flow cycles back to the state it had before the shock hit. The time evolution is thus one in which the vane circulation changes cycli-

Contributed by the International Gas Turbine Institute of ASME for publication in the JOURNAL OF TURBOMACHINERY. Manuscript received July 20, 2009; final manuscript received August 20, 2009; published online October 21, 2010. Editor: David Wisler.

[1]The code used for the unsteady simulations, which are both three-dimensional and two-dimensional, was MSU TURBO.

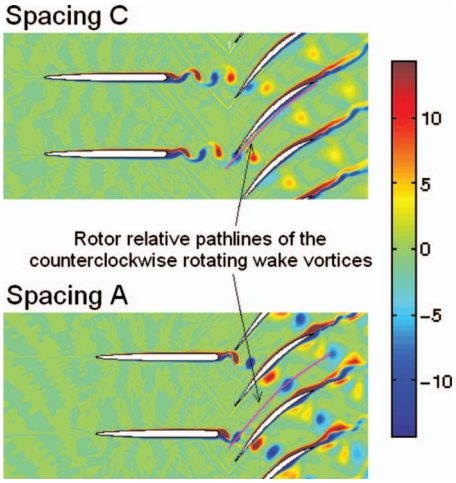

Fig. 1 Vorticity contours at midspan in SMI IGV-rotor configuration at two different interbladerow spacings. The pink line shows the path of the counterclockwise rotating vortices in the rotor frame.

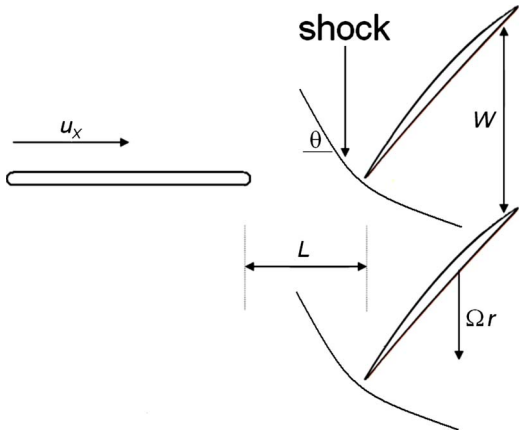

Fig. 2 Relative position of vane and rotor at time $t=0$

cally during a rotor passing, with the consequence that the vortex sheets of opposite signs are shed and rolled up into two counter rotating vortices.

The solid pink lines in the upper and lower computational results shown in Fig. 1 indicate, for two given vortex positions at the leading edge plane, the connection with vortices shed at an equivalent time in the previous shedding cycle. The solid lines thus give information about the overall trajectory (a pathline in the rotor reference frame) of a vortex within the blade passage. In addition to the difference in strength between the configurations, Fig. 1 shows that the trajectory of the vortices in the rotor is different for spacings A and C. The change in location of the trajectory with respect to the rotor blades, which is critical to changes in rotor work input, will be referred to as a change in the *wake phase*.

Zachcial and Nuernberger [11] used numerical simulations to illustrate that for a rotor downstream of a stator, a change in the wake phase can have an effect on the rotor efficiency. Their conclusion was that compressor efficiency was greatest when the vortices were positioned such that the suction side boundary layer edge velocity was reduced. The current research has a different focus, specifically the mechanism responsible for the change in the work input and peak pressure rise due to wake phase change. The purpose of this paper is to quantify the resulting change in the work input, explain the fluid dynamic reasons for the change, and provide guidelines for determining the wake phase for beneficial effects. Further, the effect of wake phase on the tip clearance flow and the subsequent changes in peak pressure rise will also be addressed within the context of the mechanism that is described.

2 Quantification of Wake Phasing

2.1 A Nondimensional Wake Phasing Parameter. To discuss the changes in the rotor performance due to changes in the vane wake phase, it is useful to introduce a nondimensional parameter, referred to here as B_3 [12], which quantifies the wake phase. Changes in B_3 are associated with changes in the vortex trajectory. Figure 2 depicts the geometry used to describe the parameter. Time $t=0$ is defined to be when the leading edge of the rotor blade is at the same pitchwise location as the vane being observed. (This sets the reference for the phasing measurement.) B_3 represents the ratio of the time when the next vortex pair shed by the vane enters the rotor passage to the time for the rotor to move one pitch. Larger values of B_3 mean the position of vortex entry into the rotor passage moves away from the suction surface.

The time that the vortex pair shed by the vane enters the rotor passage, in relation to the time origin $t=0$, is composed of the time for the shock to impact the trailing edge of the vane plus the time for the vortex to convect from the vane trailing edge to the rotor inlet plane. The first of these is approximately

$$t_{\text{shock\_impact}} = L\frac{\tan\theta}{\Omega r} \tag{1}$$

where L is the length of the interbladerow gap, θ is the angle the rotor bow shock makes with the axial direction, and Ωr is the rotor wheel speed at radius r. Impingement of the shock on the vane trailing edge causes the vortex shedding that results in the formation of a wake vortex pair, and the shedding is therefore assumed to also occur at time $t_{\text{shock\_impact}}$. With u_x as the axial velocity, the time for this vortex pair to convect across the interbladerow gap is

$$\Delta t_{\text{convect}} = \frac{L}{u_x} \tag{2}$$

The time at which the vortex pair enters the rotor passage t_1 is thus

$$t_1 = t_{\text{shock\_impact}} + \Delta t_{\text{convect}} = L\frac{\tan\theta}{\Omega r} + \frac{L}{u_x} \tag{3}$$

The time for the rotor to move one rotor pitch is

$$t_2 = \frac{W}{\Omega r} \tag{4}$$

where W is the rotor pitch. The B_3 parameter is the ratio of the two times t_1 and t_2, so with ϕ the flow coefficient

$$B_3 = \frac{L}{W}\left(\frac{\Omega r}{u_x} + \tan\theta\right) = \frac{L}{W}[(1/\phi) + \tan\theta], \tag{5}$$

A change in B_3 of unity corresponds to a change in the wake phase of 2π radians (360 deg), or, equivalently, a pitchwise shift in the wake vortex path of one rotor pitch. This means that values of B_3 that are whole numbers apart (e.g., 1.4 and 2.4) represent the same wake phase with the vortices following the same trajectory through the rotor.

2.2 Numerical Experiments on Effects of Wake Phasing. Initial three-dimensional simulations showed that the effects of interest occurred over the whole blade span and, except near the tip and hub, the central mechanism could be described in two-dimensional terms. A two-dimensional unsteady numerical experiment was thus carried out to evaluate the effect of changes in the

Table 1 2D compressor parameters

Parameter		Value
Inlet M_{rel}		1.21
Aspect ratio		0.961
Gap at 65% span (fraction of rotor pitch)	Far	1.22
	Mid	1.09
Rotor stagger angle (deg)		45.9
D factor at design		0.535
Stagnation pressure ratio at design		1.75
IGV-to-rotor ratio		2/3
D factor hub		0.545

wake phase on the rotor performance. In this, one requirement of the conditions simulated was that there should be a substantial difference in the phase of the IGV wake shedding compared with changes in the strength (i.e., size and circulation) of the wake vortices, so that the computed changes in the compressor performance are clearly the result of the change in the wake phase. A specific difficulty is that the upstream pressure field decays with axial distance, and thus, the spacings examined must be chosen to minimize the effect of this decay. This can be addressed by using a large spacing, although then the effect itself is small. Some trials and errors showed that appropriate parameters for the experiment could be obtained using spacing C and modifying it to create a change in B_3 of 0.42.

MSU TURBO [13], which is the solver used in this numerical experiment, was employed with phase-lag boundary conditions applied on the tangential boundaries of the blade passages [14]. To ensure that the calculations adequately capture the key features of the compressor flow field, the grid density distribution and calculation procedure were chosen to match the numerical experiments done by Gorrell et al. [15,2]. In that study, computations showed good agreement with both stage performance metrics (total pressure ratio and efficiency) and particle image velocimetry (PIV) data from physical experiments. The evidence is thus that the grid density, numerical timestep, and sampling rate are appropriate for the current paper.

The geometries examined consisted of two IGV-rotor configurations. A section of the SMI rotor at 65% span was used as the representative geometry. The parameters of the two-dimensional geometry are shown in Table 1. The only difference between the two configurations was the change in the interbladerow spacing. The first configuration, which is referred to as "Far," has interbladerow spacing equal to configuration C at the 65% span, which is 1.22 times the rotor pitch. The second configuration, which is referred to as "Mid," has an interbladerow spacing reduced by 11–1.09 pitch. The difference in B_3 between the two configurations is 0.42, implying a change in phasing of 2.64 rad (151 deg) and a shift of the vortex path by nearly one-half pitch in the circumferential direction. The change in the wake path is depicted in Fig. 3; the pink line showing the rotor relative path of the counterclockwise rotating vortices is much closer to the blade pressure surface in the Far case than in the Mid case. In Fig. 3, and throughout this paper, vorticity is normalized by the freestream axial velocity divided by rotor pitch. (This quantity can be interpreted as a rough measure of blade circulation per unit area.)

As mentioned, an objective was to ensure minimal change in the vortex strength entering the rotor in the two configurations. A simple measure for nonuniformity in the entering flow is given by the root mean square value of a perturbation velocity, defined as

$$u' = \sqrt{(u_x - \overline{u_x})^2 + (u_y - \overline{u_y})^2} \tag{6}$$

where the overbars represents the pitch- and time-averages of the velocity components. The metric $0.5\rho u'^2$ is an approximation for the stagnation pressure drop that would occur if the wake were to mix out at constant pressure [12]. Averaging this metric over the

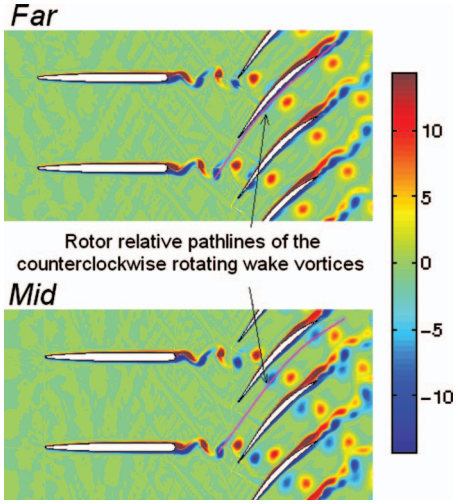

Fig. 3 Vorticity contours in two-dimensional SMI IGV-rotor configuration at two different interbladerow spacings. The pink line shows the path of the counterrotating vortices in the rotor frame. The Far geometry has an axial gap of 122% of the rotor pitch, while the Mid geometry has an axial gap equal to 109% of the rotor pitch.

pitch and in time, and nondimensionalizing by the inlet dynamic pressure gives an approximate measure for nonuniformity as

$$\frac{\overline{0.5\rho u'^2}}{p_{t\_\text{inlet}} - p_{\text{inlet}}} = \frac{\frac{1}{\tau}\frac{1}{A_{\text{total}}}\int\left[\int 0.5\rho u'^2 dA\right]dt}{p_{t\_\text{inlet}} - p_{\text{inlet}}} \tag{7}$$

At the rotor inlet, there is a 0.2% difference in this quantity between the two configurations, demonstrating the objective has been achieved because the pitch-averaged, time-averaged, flow that enters the rotor passage is nearly identical in both configurations. As will be shown, however, the differences in the metric of Eq. (7) at the rotor trailing edge are two orders of magnitude larger (23%), showing that the *processing* of the two "identical" inlet flows is much different, because of the difference in wake phase.

2.3 Impact of Wake Phasing on Time-Mean Performance. Time-mean adiabatic efficiency and rotor stagnation temperature rise from the unsteady calculations are shown in Fig. 4 The adiabatic efficiency and stagnation temperature rise are defined using mass-averaged (over time and over the passage area) values of stagnation temperature and stagnation pressure. The stagnation temperature rise across the rotor is normalized by the inlet stagnation temperature, and the corrected mass flow is normalized by the inlet corrected mass flow of the isolated rotor at choke conditions. The goal was to make the performance comparison at the corrected mass flow corresponding to design conditions (mass flow of 0.97). The back pressure was incrementally changed until data points at the design mass flow were attained. All the data points obtained in this process are shown in Fig. 4. At the corrected mass flow of 0.97, the work input of the rotor in the Far configuration was 3% greater than that of the Mid configuration. The efficiency change in the Far configuration was small, which is 0.1 points greater than that of the Mid configuration, and, as mentioned in Sec. 1, is not addressed further in this paper.

At the rotor exit the nonuniformity metric defined in Eq. (7) was 23% higher for the Mid configuration than for the Far configuration. This indicates a large difference in the behavior within the passage for the two configurations. In Sec. 3, we link this difference to the change in the wake phase through quantitative analysis and arguments concerning the physical mechanisms.

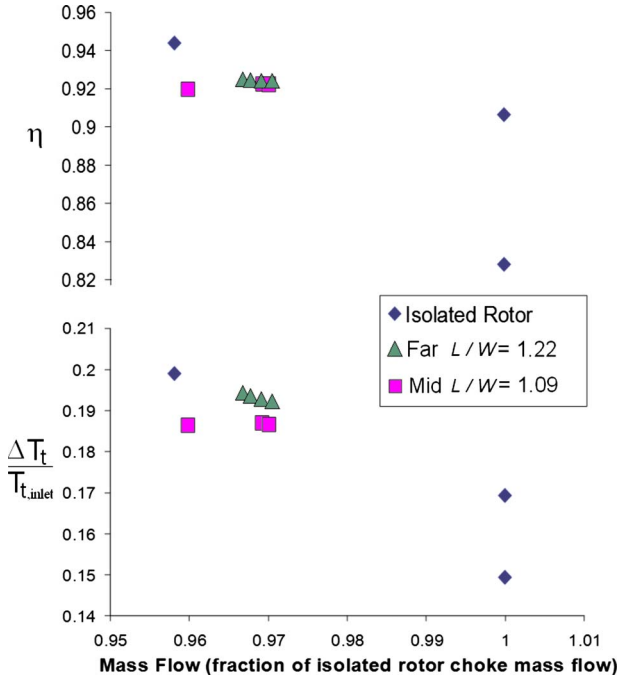

Fig. 4 Efficiency and stagnation temperature rise versus mass flow for Far and Mid geometries

3 Defining the Time-Mean Footprint of IGV Shed Vortices

3.1 Steady Flow Representation. To understand the time-mean footprint of the IGV wake vortices and, more importantly, the relation of this footprint to the change in rotor performance, we consider the vortices in both an unsteady and a steady representation, as depicted in Fig. 5. Each IGV sheds counter rotating vortices which move through the rotor as illustrated in Fig. 5(*a*).[2] The rotor relative path of the counterclockwise rotating vortices are denoted by the dotted lines. The vortices along this line in Fig. 5(*a*) have been shed from different IGVs and have entered the rotor passage at different times.

The time-mean relative stagnation pressure variation associated with the presence of the vortices is described by Crocco's theorem applied in the rotor reference frame. If we denote the difference between the instantaneous velocity and the time-mean velocity by u', and the instantaneous vorticity by ω' (the time-mean vorticity is zero), we can write an expression for the variations in the time-mean stagnation enthalpy and in entropy as

$$\overline{u' \times \omega'} = \nabla \overline{h_t} - \overline{T \nabla s} \tag{8}$$

where the overbar denotes a time-mean. The entropy associated with the shed vortices is concentrated in "entropy spots," whose centers are close to the vortex center (within roughly 10% of the vortex diameter). Outside of these regions the entropy is uniform and ∇s is zero. The time-mean relative stagnation pressure outside the high entropy regions is[3]

$$\overline{u' \times \omega'} = \nabla \overline{h_t} = \overline{\left(\frac{\nabla p_t}{\rho_t}\right)} \approx \frac{\nabla \overline{p_t}}{\rho_t} \tag{9}$$

[2]In the actual numerical experiment the spacing between IGVs is larger than that of the rotor, but additional rows of vortices are drawn in the figure to help make the arguments more transparent.

[3]This can also be argued using the Euler turbine equation referred to the vortices that move through the blade passage [7]. For a row of vortices of circulation Γ per unit length of the row, moving with speed u_v, the stagnation enthalpy difference across the row is Γu_v.

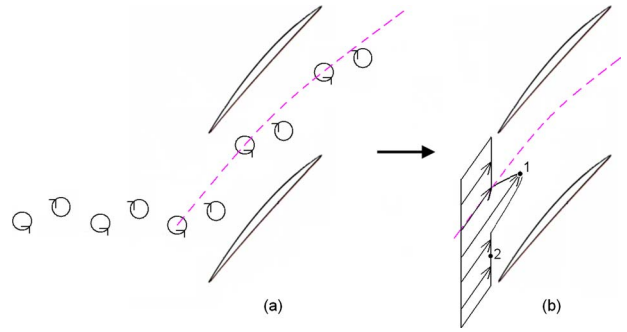

Fig. 5 Unsteady vortex flow field and time-mean representation. The dotted line shows the path of the counterclockwise rotating vortices in the rotor frame. In 5b, label "1" denotes fluid with high relative stagnation pressure, while label "2" denotes fluid with low relative stagnation pressure.

The approximation implied by Eq. (9) is that the time-mean flow of the unsteady wake vortices that enter the rotor can be viewed as a steady, pitchwise nonuniformity in relative stagnation pressure, as sketched in Fig. 5(*b*), with the fluid at label "1" having a higher relative stagnation pressure than that at label "2." Quantitative demonstration of the correspondence is given by the contours of time-mean relative stagnation pressure in the rotor reference frame in Fig. 6, which have been extracted from unsteady calculations for the Far and Mid configurations. The values of relative stagnation pressure in Fig. 6, and throughout this paper, have been normalized by the ambient absolute stagnation pressure.

The message of the above is that the change in the vortex trajectory between the two configurations appears in the time-mean flow field as a change in the pitchwise location of the regions of high and low relative stagnation pressures. Changes in the wake phase relative to the rotor change the relative stagnation pressure of the fluid directly adjacent to the rotor, influencing the capability of the boundary layers to negotiate the rotor pressure rise. Specifically, the lower the relative stagnation pressure fluid

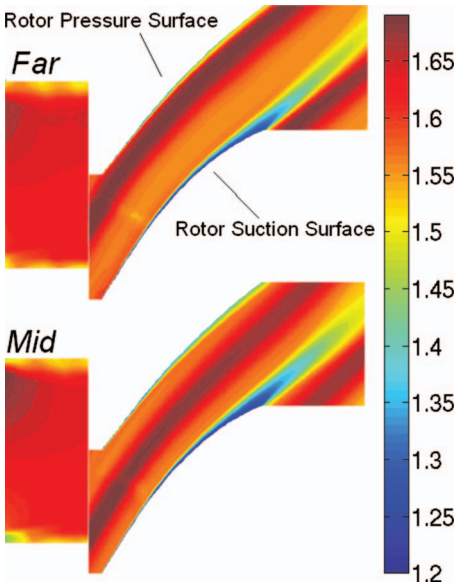

Fig. 6 Time-mean relative stagnation pressure contours for Far and Mid geometries extracted from unsteady computations. The Far geometry has a vane-rotor axial gap equal to 122% of the rotor pitch, while the Mid geometry has an axial gap equal to 109% of the rotor pitch.

that encases the rotor, the larger the exit boundary layer displacement thickness and the deviation.

The point can be made explicit using the momentum integral equation written as

$$\frac{d\theta}{ds} - (H+2)\frac{\theta}{\rho u_E^2}\frac{dp}{ds} = \frac{C_f}{2} \tag{10}$$

The computations to be described show the pressure rise in the rotor changes by less than 5% as a result of the wake phasing. To motivate the arguments, therefore, we couch the discussion in terms of how the response of the momentum and displacement thickness to a given pressure gradient is affected by changes in the boundary layer edge velocity. It is emphasized, however, that this discussion should be regarded as a plausibility argument only; the calculations that have been conducted furnish direct quantitative evidence for the magnitude of the changes observed.

The boundary layer edge velocity u_E in Eq. (10) is dependent on the relative stagnation pressure of the fluid adjacent to the blade. Referring to Fig. 5(*b*), the fluid at label 1 would result in a greater edge velocity (if placed at the blade surface) than the fluid at label 2. For the flows of interest, the inviscid distortion of the boundary layer velocity is more important than the effect of skin friction so we neglect the term on the right hand side of Eq. (10). Doing this, and using a mean value for the boundary layer shape factor (from the calculation, for example), the change in the displacement thickness between arbitrary stations 1 and 2 is found as

$$\frac{\delta_2^*}{\delta_1^*} = \exp\left\{(H_{\text{mean}}+2)\int_1^2 \frac{dp}{\rho u_E^2}\right\} \tag{11}$$

For a given pressure rise from any station 1 to station 2, Eq. (11) indicates that a lower boundary layer edge velocity results in a larger fractional change in the displacement thickness. (Again, Eq. (11) should be regarded as a plausibility argument only; the quantitative evidence is from the computations to be described.) Larger exit displacement thickness means lower pressure rise (mitigating the strict interpretation of Eq. (11) although not the qualitative conclusion) and lower work done by the rotor, compared with the situation when the rotor is encased in high relative stagnation pressure fluid.

To summarize the arguments given, first, from Eq. (9), an increase in the wake vortex circulation results in an increased time-mean nonuniformity in relative stagnation pressure, and thus, the variation in boundary layer edge velocity as a function of wake phasing. Equation (11), then, implies a larger displacement thickness when the phase of the time-mean profile is such that the lower relative stagnation pressure fluid encases the blades. Having presented these qualitative arguments, we now examine in more depth the time-mean and unsteady computations of the flow in the IGV-rotor combination.

3.2 Steady Flow Computations of Wake Phasing Impact. We now examine the result of a steady computation to evaluate the ideas that have been described. The time-mean flow profile from the unsteady MSU TURBO computations, which is evaluated at a station 10% of the axial chord upstream of the rotor, was used as the inlet condition for the flow through an isolated rotor, and computed using the code in a steady-state mode. The time-mean inlet profile used was moved at the same tangential speed as the rotor, so the flow was steady in the frame of the rotor. Calculations were performed with the profile at three different pitchwise positions, equally spaced across the rotor pitch, to assess the effect of position of the steady inlet profile, relative to the rotor, on the work input. Figure 7 gives the results as plots of stagnation temperature rise, i.e., work input versus mass flow. It is seen that the rotor work input at a given mass flow is dependent on the position of the inlet flow profile. Further, a more detailed examination will show that for a given corrected mass flow, the work input is largest when the suction side is bathed in the fluid with the highest

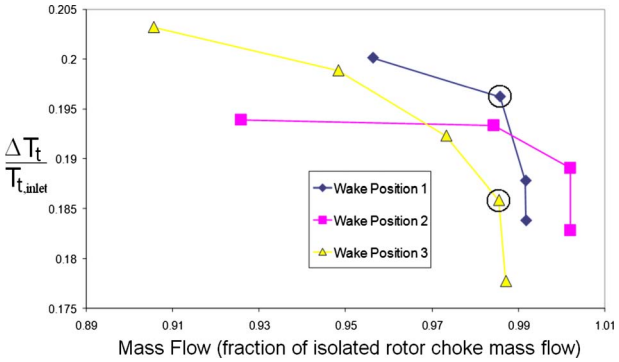

Fig. 7 Stagnation temperature rise versus mass flow from steady computations. The relative stagnation pressure contours corresponding to the circled data points are shown in Fig. 8.

relative stagnation pressure, as implied by the arguments in Sec. 3.1.

Figure 8 shows the relative stagnation pressure contours throughout the rotor passage for wake positions 1 and 3, both at a corrected mass flow of 0.986, corresponding to the circled data points in Fig. 7 The upstream stratification in relative stagnation pressure places the blade within the high relative stagnation pressure region for position 1 and within the low relative stagnation pressure region for position 3. In the former situation, the suction side boundary layer has a smaller displacement thickness and smaller deviation angle than in the latter. As a result, the pressure rise and flow turning are both higher when the profile is in position 1, leading to a 5.3% higher work input than when the profile is in position 3. Figure 7 also shows that the wake position that results in the largest work input changes with the corrected mass flow. Even though the position of the profile at the domain inlet is fixed for a given "wake position" case, the axial velocity in the freestream is a function of the inlet mass flow, which means that the B_3 parameter for a given "wake position" case is also a function of the inlet mass flow.

The model calculations are, to a good approximation, independent of the relative stagnation temperature distribution at the inlet provided that the relative stagnation pressure distribution is un-

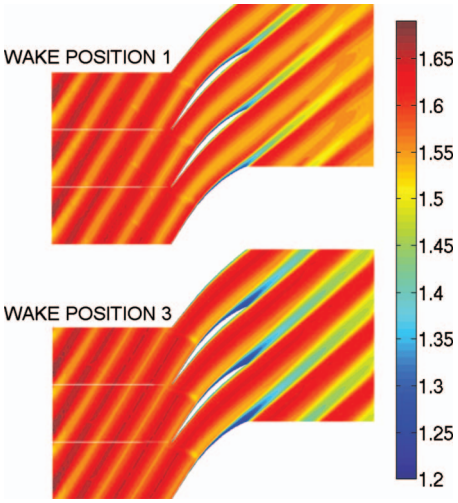

Fig. 8 Relative stagnation pressure contours for wake position 1 (high relative stagnation pressure fluid over blade) and wake position 3 (low relative stagnation fluid over blade). These contours correspond to the circled data points from Fig. 7.

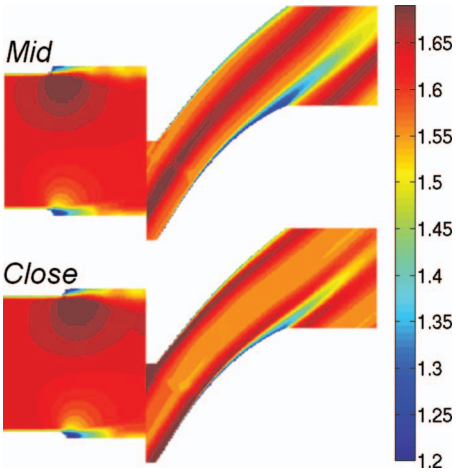

Fig. 9 Time-mean relative stagnation pressure contours for Mid and Close geometries. The Mid geometry has a vane-rotor axial gap equal to 109% of the rotor pitch, while the Close geometry has an axial gap equal to 95% of the rotor pitch.

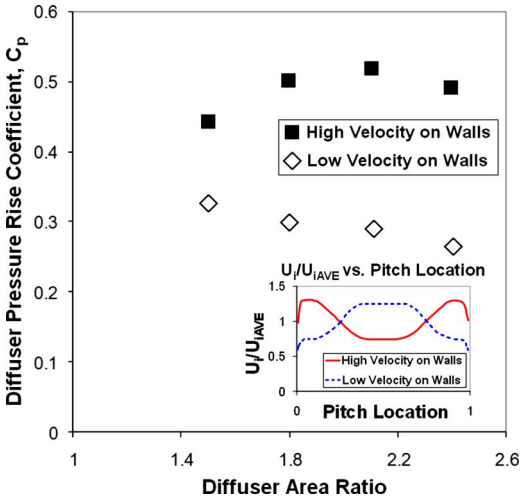

Fig. 10 Diffuser pressure rise coefficient C_p versus the diffuser area ratio for two different inlet velocity profiles. The inlet profiles are shown in the inlay figure.

changed [7]. Calculations were carried out with both uniform stagnation temperature and isentropic flow (and thus a varying stagnation temperature) at the inlet, which bound the situations of interest. The computed variation in rotor work due to changes in the wake phase was similar for both temperature distributions, with the *maximum* difference in the variation being 12% of the variation itself.

3.3 Potential Beneficial Effects of Wake Phasing. In Sec. 1 of this paper, we referred to previous work that showed an adverse effect from moving a transonic rotor and inlet guide vane closer together. The ideas presented here imply that this need not be the situation in all cases, and in this section, we define guidelines for a potentially beneficial interaction. In interpreting the results, we again mention that there are two effects at work. One is phasing. The other is that the static pressure variations seen by the upstream vane row, and hence, the strength of the shed vortices, increase as the distance to the rotor is decreased. The criterion for differentiating between the two is that the change in the pressure field decay is small over a spacing change that corresponds to a change in the wake phasing of (roughly) 180 deg, so that the wake phasing is the major driver. This is the case between the Far and Mid configurations described in Secs. 2.2 and 2.3.

Using the two-dimensional IGV-rotor configuration, the reduction in spacing (compared with the Mid spacing configuration) necessary to result in a beneficial wake phase was determined as follows. The location of the peak relative stagnation pressure for the Mid spacing is near the midpitch (0.45 pitch from the suction surface), representing a wake phasing that produces the lowest rotor work. The B_3 parameter thus needs to be reduced by 0.45 (162 deg of phase) to move the peak relative stagnation pressure fluid to the suction surface. This was achieved by a decrease in IGV-rotor spacing of 13%, resulting in an IGV-rotor spacing of 0.95 rotor pitch, referred to below as "Close."

Calculated contours of the time-mean relative stagnation pressure corresponding to the Mid and Close spacing calculations are shown in Fig. 9. It can be seen that the suction side boundary layer is smaller in the Close configuration than in the Mid configuration even though the relative stagnation pressure nonuniformity is larger for the former (peak-to-peak variations of 16.2% and 15.9% of the inlet dynamic pressure, respectively). The altered phasing leads to a 4% increase in rotor work.

3.4 Impact of Inlet Velocity Profile on Diffuser Performance. The trend of reduced work input when the low relative stagnation pressure fluid is adjacent to the rotor is consistent with two-dimensional straight channel diffuser experiments conducted by Wolf and Johnston [16,17]. In the experiments, a square wave inlet velocity profile was used to provide two different situations: (i) high velocity in the center of the diffuser and low velocity at the walls, and (ii) low velocity at the center of the diffuser and regions of high velocity at each wall. Figure 10 illustrates the differences in the diffuser static pressure rise coefficient (rise in static pressure normalized by the inlet dynamic pressure) with the two inlet profiles, for several diffuser area ratios from 1.5 to 2.4. The inset within Fig. 10 shows the profiles of the inlet velocity, normalized by the average inlet velocity, versus the pitch location, where locations of 0 and 1 correspond to the diffuser walls. With high velocity, i.e., high stagnation pressure, adjacent to the diffuser walls, the diffuser pressure recovery was from 36% to 86% higher (depending on the diffuser area ratio) than with the low velocity region near the wall. A control volume analysis given in the Appendix shows that the differences in the diffuser pressure rise are in qualitative correspondence with the circumferential force changes seen in the numerical experiments presented here.

3.5 Connection With Clocking. We have presented physical arguments and computations showing that phase-locked shed vortices can be viewed as having a time-mean influence on the relative stagnation pressure profile entering the rotor. A further implication is that the effect of changes in the wake phase is similar to the effect of changes in *clocking*. Clocking refers to the pitchwise relative positioning of two blade rows with the same wheel speed, i.e., two rows of stators or rows of rotors on the same shaft. The path of the wake from an upstream stator through the downstream stator will depend on the geometry. Changes in clocking change this path, and therefore, the performance of the downstream blade row. Key et al. [18] found that the flow in the downstream stator of a highly loaded stage was separated when the wake from an upstream stator impinged upon it, leading to reduced efficiency. Although, as has been mentioned, the current research focuses on work input rather than efficiency, the results of that study are consistent with the ideas presented in this paper.

4 Flow Parameter Scaling of Wake Phasing

4.1 Effects of Inlet Mach Number and Inlet Relative Stagnation Pressure Nonuniformity. Given that the presence of a time-mean stagnation pressure nonuniformity can be the result of wake phasing (as well as clocking), it is of interest to determine the effect of relevant flow parameters. Specific questions are the impact on rotor work of: (i) the inlet relative Mach number, and

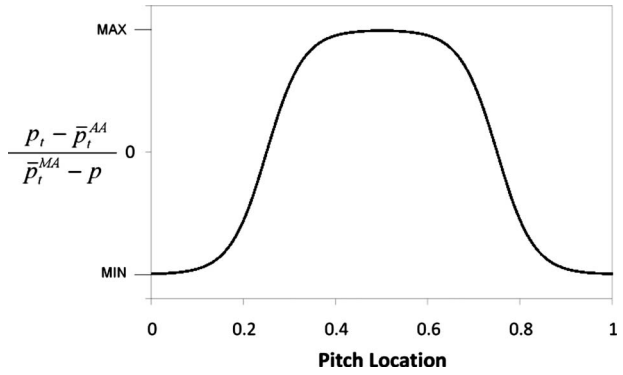

Fig. 11 Rotor inlet nominal stagnation pressure nonuniformity (based on the time-mean of the unsteady computations)

(ii) the amplitude of relative stagnation pressure nonuniformity. To answer this, a series of steady computations have been carried out. In these parametric studies, all quantities reported are in the rotor relative frame. The results are presented in terms of changes in the circumferential component of the blade force as a function of the inlet profile phase, for different inlet Mach numbers and inlet relative stagnation pressure nonuniformity amplitudes. A fractional change in the circumferential component of the blade force translates to the same fractional change in the work input.

The MISES code [19][4] was used for the parametric studies because it afforded greater control in maintaining a constant corrected mass flow at which to compare the different cases. The inlet stagnation temperature and the turbulence intensity were uniform and the blade geometry was a representative transonic airfoil taken from the literature (a German Research and Test Center for Air and Space Flight (DFVLR) cascade) [20]. The relative stagnation pressure profile used is shown in Fig. 11. The profile is composed of hyperbolic tangents, such that the profile is a "rounded square wave," as is characteristic of time-mean relative stagnation pressure profiles from phase-locked vortices. The results should therefore be generic for the range of Mach numbers and amplitudes shown.

To describe the amplitude of the stagnation pressure nonuniformity, we define a nondimensional parameter (DPT) as the peak-to-peak difference in stagnation pressure divided by the mass-averaged dynamic pressure at the inlet station

$$\mathrm{DPT} = \left(\frac{p_{t,\max} - p_{t,\min}}{\bar{p}_t^{\mathrm{MA}} - p} \right)_{\mathrm{inlet}} \tag{12}$$

The nondimensional coefficient used to describe the circumferential force is the delta force coefficient (DFC) defined as

$$\mathrm{DFC} = \frac{F_\theta - \bar{F}_\theta}{(\bar{p}_t^{\mathrm{MA}} - p)_{\mathrm{inlet}}} \tag{13}$$

The quantity F_θ is the circumferential force on the blade per unit inlet flow area and $\bar{F}_\theta$ is the circumferential force per unit inlet flow area for a uniform inlet profile. DFC is zero for a uniform inlet stagnation pressure.

Figure 12 shows the nondimensional blade force (DFC) as a function of the pitchwise position of the peak in the stagnation pressure for different amplitudes of the inlet stagnation pressure profile (different DPT). For all scatter plots presented, a pitch location of 0 refers to the rotor pressure surface and pitch location of 1 refers to the suction surface. The ordinate in the figure is

[4]In order to specify a nonuniform stagnation pressure at the inlet, a modified version MISES was used. Professor Mark Drela provided instruction for these modifications.

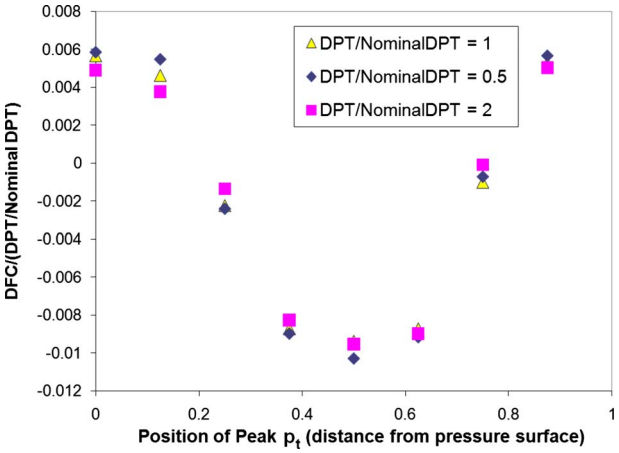

Fig. 12 Circumferential force variation (DFC) versus the pitchwise position of inlet stagnation pressure profile for different amplitudes of inlet nonuniformity

DFC/(DPT/Nominal DPT). The three data sets correspond to different values of inlet DPT normalized by the "Nominal DPT" of 0.16, which is the value obtained from the unsteady MSU TURBO calculations. The triangles are for a normalized value equal to unity (i.e., the value seen in the unsteady calculations), the diamonds are for a value half of unity, and the squares for a value twice of unity. All the calculations are for an inlet Mach number of 0.5.

The trends seen in these steady computations are consistent with the results from the unsteady calculations in that the largest circumferential force is obtained when the fluid with highest relative stagnation pressure encases the blade. The good correspondence between the different normalized stagnation pressure nonuniformities shows that the sensitivity of rotor work to changes in the wake phase is roughly linear with DPT over the range investigated.

Figure 13 shows the nondimensional blade force (DFC) as a function of the pitchwise position for five different inlet relative Mach numbers. A Prandtl–Glauert compressibility correction has been applied to DFC. The data for all the subsonic inlet Mach numbers show a tight grouping, indicating the scaling of the circumferential force component with the Prandtl–Glauert factor of $1/\sqrt{1-\mathrm{M}^2}$. The data for supersonic inlet flow (M=1.15) does not collapse with the other data sets, although the dependence on the pitchwise location of the profile is essentially the same as that for

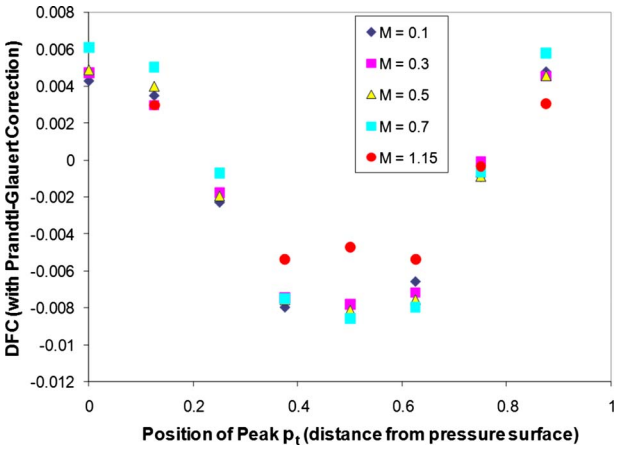

Fig. 13 Circumferential force variation (DFC) versus the pitchwise position of inlet stagnation pressure profile for different rotor inlet Mach numbers

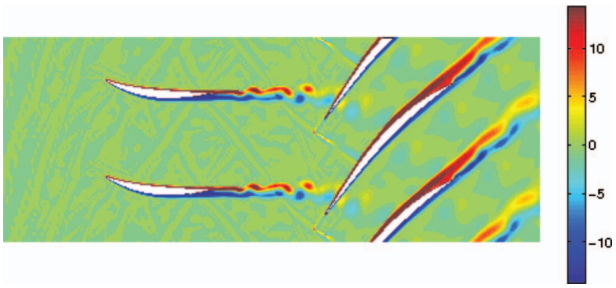

Fig. 14 Vorticity contours for SMI deswirler-rotor geometry

the subsonic inflow Mach numbers. One possible reason for the difference in magnitude is a decrease in amplitude of the stagnation pressure nonuniformity as the flow passes through the shock.

The calculations in Figs. 12 and 13 both show the scaling of the wake phasing effect and confirm that the steady computations capture the effect of changes in the wake phasing on rotor work input. The results in Fig. 12 are thus applicable to the unsteady calculations described earlier for the Far and Mid configurations. The Far case corresponds to a peak relative stagnation pressure position of approximately 0.2, and the Mid case to 0.55. Therefore, Fig. 12shows that the difference between DFC values for the Far and Mid cases should be approximately 0.008 (the difference in ordinate between abscissae of 0.2 and 0.55). The actual difference in DFC value between the Far and Mid unsteady TURBO calculations was 0.0089, which is close to this estimate.

4.2 Effect of Vane Trailing Edge Thickness. For wake phasing to have a measurable impact on the rotor performance, the vane must shed counter-rotating vortices that are phase-locked to the rotor and that create a level of time-mean relative stagnation pressure nonuniformity of engineering interest.[5] For this to occur, there needs to be a strong interaction between the rotor-induced static pressure field and the upstream vane, as is the case when the rotor is transonic and a rotor bow shock is present. There are also geometric requirements for such a wake to exist, because the counter-rotating vortices shed behind a vane with thick trailing edge will have greater circulation than those for the same shock but a vane with a thin trailing edge.

To show the magnitude of this effect, calculations were carried out with the axial IGV replaced with a deswirler vane row that had been designed to be used in the SMI facility with swirling flow upstream of the vane [21]. The design swirl angle upstream of the deswirler was 29 deg, with the exit flow being turned to the axial direction.

In these calculations, the number of grid cells was increased and the grid density distribution altered to increase the resolution near the deswirler trailing edge. Additionally, a grid study was performed in which the number of cells in the deswirler grid was quadrupled (by doubling the cell density in the axial and circumferential directions). The change in grid resulted in a change in the DPT of less than 8% in the deswirler-rotor configuration, indicating that the cell density in the nominal deswirler grid was adequate to capture the features related to wake phasing.

The deswirler has a much thinner trailing edge than the original axial inlet guide vanes (0.0155 versus 0.111 rotor pitch, respectively). In accord with the mechanism postulated by Gorrell et al., the magnitude of the shed circulation will be greatly reduced. Figure 14 which can be compared with Fig. 3, shows the deswirler wake and the passage through the rotor; there are qualitative differences between the vortex configurations and strengths in the two figures.

[5]The specific cutoff depends on the eventual use of the measurement, but values of DPT that caused work input changes that were below a tenth of a percent, say, would be below such a threshold.

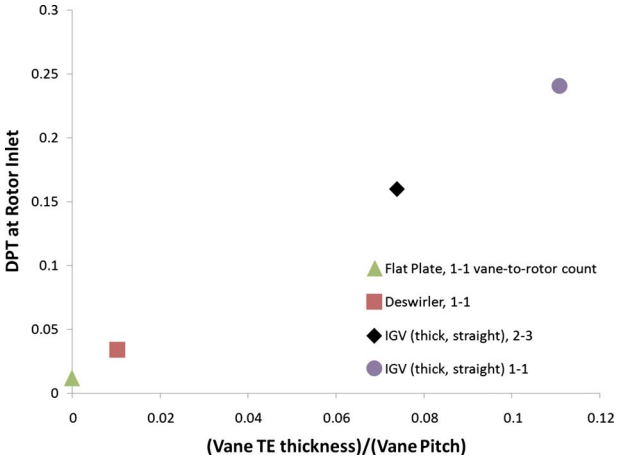

Fig. 15 Amplitude of relative stagnation pressure profile versus vane trailing edge thickness/vane pitch. The same interbladerow spacing ($L/W=1.22$) was used for all data points in this plot.

Figure 15 gives a direct view of the effect of trailing edge thickness on the amplitude of the rotor inlet relative stagnation pressure nonuniformity. The four points correspond to calculations with the flat plate IGV, two original (thick) IGVs with different pitchwise spacings, and the deswirler. All the calculations are carried out for the same axial spacing from vane trailing edge to rotor (1.22 rotor pitch). There is an order of magnitude difference between the time-mean relative stagnation pressure nonuniformity presented to the rotor with the flat plate and with the thick IGV. The deswirler creates a larger nonuniformity than the flat plate, but is still a factor of five or so below the thick IGV with vane-to-rotor blade count of 2 to 3. The calculations show that the amplitude of the time-mean relative stagnation pressure nonuniformity at the rotor inlet is roughly proportional to vane trailing edge thickness divided by the vane pitch, although there may be additional parametric dependencies as well. Additional investigation of high-fidelity three-dimensional calculations of a swirler/deswirler/rotor geometry performed by List et al. [21] also indicated that a small ratio of trailing edge thickness to vane pitch leads to a reduced time-mean relative stagnation pressure nonuniformity.

5 Effects of Wake Phasing on Rotor Tip Clearance Flow and Pressure Rise

5.1 Mechanism for Potential 3D Effects and Numerical Experiment Setup. The discussions so far have been about effects that can be viewed as two-dimensional. There can, however, be consequences of the creation of a stratified relative stagnation pressure field, which are three-dimensional in nature and qualitatively different from those mentioned. An example described in this section is the effect of wake phasing can have on the tip clearance flow, and hence, on the maximum pressure rise capability of a compressor.

We have shown that the time-mean relative stagnation pressure nonuniformity resulting from wake vortices can be positioned to alter compressor work input. For tip clearance flow, this positioning can also affect peak pressure rise capability, and possibly, the operating range. The link is through the clearance vortex, which is a major contributor to rotor exit blockage, and hence, to the pressure rise limitation, and its sensitivity to relative stagnation pressure stratification. As described by Khalid et al. [22], supplying the vortex core with fluid of higher relative stagnation pressure decreases the blockage at the rotor exit, and thus, increases the pressure rise capability. It is hypothesized that if the region of high relative stagnation pressure can be positioned such that

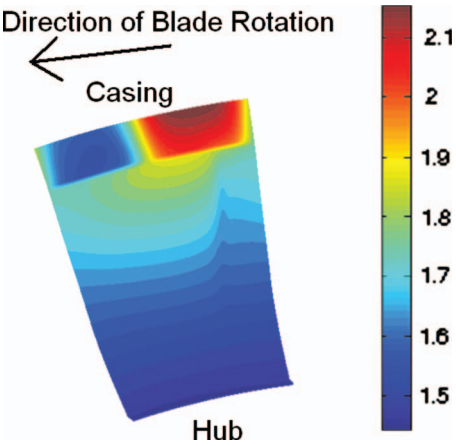

Fig. 16 Relative stagnation pressure at domain inlet for test case (stratified inlet position 1)

the high relative stagnation pressure fluid forms the core of the clearance vortex, flow stratification thus offers the potential to reduce the blockage and increase the peak pressure rise.

To assess the hypothesis, a series of three-dimensional calculations have been carried out. These calculations have been deliberately abstracted compared with the actual situation in that the profile of rotor inlet stagnation pressure does not account for the radial variation that exists near the casing, and the steady calculations do not capture unsteady perturbations in the tip vortex motion. The point of the computations in this section, however, are more qualitative than those in the rest of the paper with the objective of evaluating the plausibility of the idea that wake phasing can affect the tip clearance flow.

The specific objective of the three-dimensional steady model calculations was to define the sensitivity of rotor pressure rise to changes in the wake phase near the tip region. In the calculations, the domain inlet relative stagnation pressure in the outer 15% of the annulus was circumferentially nonuniform. For radii inboard of this value, the inlet relative stagnation pressure for the base flow was circumferentially uniform. In computing for the solution, the presence of the rotor flow field perturbs the input base flow such that the inboard region is not exactly circumferentially uniform. However, the shock-related nonuniformity below 85% span has only one-fifth of the amplitude of the imposed relative stagnation pressure near the casing, so the latter is the dominant influence. The amplitude of relative stagnation pressure nonuniformity used in the tip region was approximately three times of that observed downstream of the vanes in the unsteady SMI geometry. The large amplitude was chosen so that the effects on the tip clearance flow, and thus, the compressor performance, are readily seen.

Figure 16 shows relative stagnation pressure contours, normalized by the absolute inlet stagnation pressure, at the inlet flow plane for one of the test cases. The stratification is periodic over the rotor pitch. The pitchwise position of the relative stagnation pressure nonuniformity was shifted to evaluate the rotor performance sensitivity to profile location. The position shown in Fig. 16 is referred to as "position 1." A shift of one-quarter pitch in the direction of the rotor rotation puts the profile at "position 4," a second shift of a quarter pitch give "position 3," and another quarter pitch shift gives "position 2."

5.2 Impact of Wake Phasing Near Casing on Time-Mean Performance of 3D Rotor. The results from computations with the different relative stagnation pressure peak positions are given in Fig. 17. The figure shows the rotor pressure rise coefficient (exit static pressure minus inlet stagnation pressure, normalized by the mass-averaged inlet dynamic pressure) versus the corrected mass flow for two positions of stratified inlet profile and for a circumferentially uniform relative stagnation pressure. Position 1 is the inlet profile position that resulted in the worst near stall performance (in terms of stall flow coefficient and stagnation-to-static pressure rise coefficient), while position 3 resulted in the

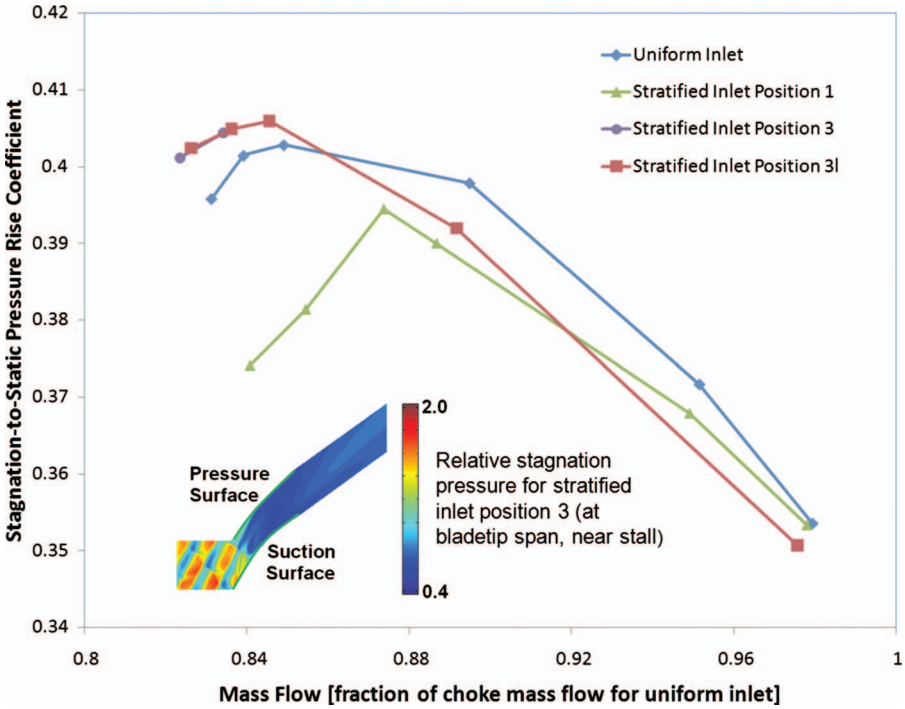

Fig. 17 Stagnation-to-static pressure rise coefficient versus mass flow. The inlay figure shows the contours of relative stagnation pressure for position 3, at the bladetip span, near stall.

best near stall performance. The calculated flow coefficient at which the rotor exhibited (a numerical) stall differed by 2.1%, and the pressure rise coefficient at near stall conditions varied by 6.8%. The reason for the performance change is the difference in the tip clearance related blockage that accompanies the change in the profile position. An additional calculation result is denoted by "position 3l," which refers to the same inlet circumferential profile as position 3, but with stratification only present in the outer 10% of the span, rather than the outer 15%. The stall flow coefficient and pressure rise coefficient at stall differed by only 0.3% compared with Position 3.

Interrogation of the computational results shows that the effective flow area at the rotor exit varied by 3.3%, depending on the stratification position. The lowest blockage occurred with the stratified flow at position 3. When the profile is in this position, the tip clearance vortex core is supplied with high relative stagnation pressure fluid, demonstrating the causal link between the blockage associated with the tip clearance flow, peak pressure rise, and upstream wake phase. There is a potential for wake phasing near the casing to affect the tip clearance flow. The implication is that if wake phasing near the casing exists, it can be used to produce a time-mean relative stagnation pressure profile that enables increased stagnation-to-static pressure rise at near stall conditions and, perhaps more importantly, mitigation of the fall off in the pressure rise and the creation of the positive slope associated with the onset of instability.

6 Summary and Conclusions

Computational and analytical studies have been carried out to determine how wake vortices, shed from an upstream vane row as the result of the rotor upstream pressure field, affect the performance of a downstream rotor. Both unsteady and steady computations have been used. The results are as follows:

- Because the shedding of the wake vortices is phase-locked to the rotor position, there is a time-mean pitchwise nonuniformity in the relative stagnation pressure entering the rotor. The relative phase of this nonuniformity affects the rotor work.
- The time-mean relative stagnation pressure of the fluid adjacent to the blade is dependent on the wake phase, which affects the rotor boundary layer thickness and the flow deviation. At a given mass flow, the maximum work and pressure rise occurs when the rotor blades are embedded in the region of high relative stagnation pressure, and the minimum work occurs when the blades are embedded in the region of low relative stagnation pressure.
- Steady computations that illustrate and explain the time-mean difference in work with wake phase have been described.
- Rotor inlet relative Mach number and amplitude of the time-mean relative stagnation pressure nonuniformity both affect the impact of wake phasing on rotor work. These effects have been quantified.
- For the cases investigated, the amplitude of the time-mean relative stagnation pressure nonuniformity that causes the wake phasing effect scales linearly with the ratio of vane trailing edge thickness to vane pitch.
- Compressor tip clearance flow can also be impacted by wake phasing. Computations are carried out, which show it is plausible that the tip clearance vortex core, and consequently, the compressor peak pressure rise (and potentially the stable flow range) can be affected by changes in the wake phase near the casing.
- Guidelines for defining the wake phasing at a given span to mitigate the negative effects on transonic rotor work have also been presented.

Acknowledgment

Support for this work was provided by AFOSR (Grant No. FA9550-05-1-0050), with Dr. T.J. Beutner, Dr. R. Jeffries, and Dr. J.D. Schmisseur as program managers. Additional support was also provided by the Co-Op program at Wright–Patterson Air Force Base. The authors would like to thank Dr. D.C. Rabe, Dr. S.L. Puterbaugh, D. Car, and M.G. List of the Air Force Research Laboratory for their help at various stages in the research project. The advice given by Professor M. Drela of MIT, Dr. J.P. Chen of Ohio State University, and Dr. N.A. Cumpsty of Imperial College is also greatly appreciated. We are grateful to the reviewers who provided insightful comments, which helped to make a more complete paper. Computational resources were provided by the Major Shared Resource Center at Wright–Patterson Air Force Base. The first author would also like to acknowledge the support of the Lemelson Minority Engineering Fellowship from the MIT School of Engineering.

Nomenclature

Letters and Symbols

- A = area
- B_3 = nondimensional wake phasing parameter
- C_p = static pressure rise coefficient
- F_θ = tangential blade force per unit inlet flow area
- H = boundary layer shape factor
- h = enthalpy
- L = interbladerow spacing
- M = Mach number
- p = pressure
- r = radius
- s = (1) entropy; (2) streamwise coordinate
- T = temperature
- t = time
- u = velocity
- (u_x, u_y) = velocity components in the Cartesian coordinates
- W = rotor pitch
- β = angle between the flow and axial directions
- Δ = change in quantity
- δ^* = boundary layer displacement thickness
- ϕ = flow coefficient
- θ = (1) angle between the rotor shock and axial direction; (2) boundary layer momentum thickness
- Ω = angular velocity
- ω = vorticity
- η = adiabatic efficiency
- ρ = density

Subscripts

- E = boundary layer edge
- exit = domain exit
- inlet = domain inlet
- t = stagnation quantity
- 1,2 = (1) station numbers; (2) numbers denoting different states

Superscripts

- AA = area-average
- MA = mass-average
- overbar (e.g., $\bar{u}$) = mean
- prime (e.g., u') = nonuniformity

Appendix: Link Between Diffusion and Blade Force

In this appendix, we present an approximate control volume analysis that links the results from the diffuser experiments of

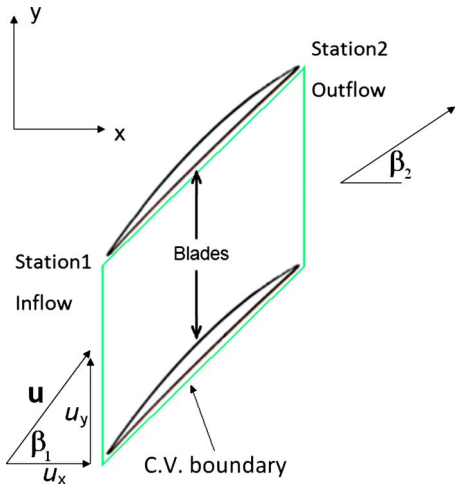

Fig. 18 Control volume used in analysis of rotor circumferential force

Wolf and Johnston [16,17] to the two-dimensional compressor calculations and shows that estimates of the reduction in the diffusion capability of the rotor, based on the diffuser results, are in rough accord with the observed reduction in the rotor circumferential force.

The control volume examined is shown in Fig. 18. The flow is taken as incompressible and two-dimensional. Station 1 is at the entrance to the rotor passage and station 2 is at the exit to the rotor passage. All quantities pertaining to this analysis are measured in the rotor relative frame.

Two effects decrease the effective flow area at exit: deviation of the flow and blockage due to boundary layer displacement thickness. For simplicity, we examine these separately. As in Fig. 19, we refer to the situation in which the deviation at the exit is significant in changing the effective flow area, but the blockage is insignificant, as "case 1," and to the situation in which the deviation at the exit is insignificant, but the blockage is significant, as "case 2." In both cases, it will be shown that the reduction in the pressure rise results in a smaller circumferential blade force.

The circumferential blade force component is equal to the net change in the circumferential momentum flux across the blade row. The ratio of exit to inlet circumferential momentum per unit span is given in Eq. (A1), which, using continuity, can be expressed as

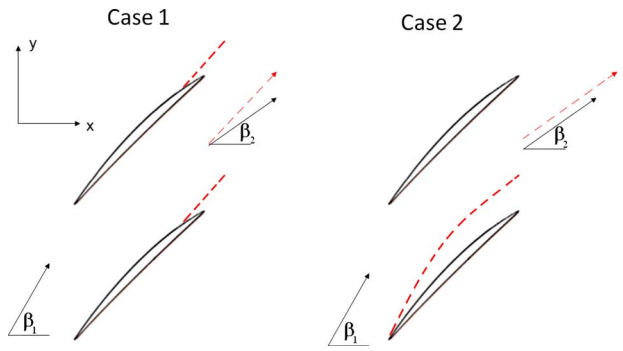

Fig. 19 Decrease in the exit area in a blade passage. The dotted line coming off the suction surface represents the edge of the suction side boundary layer. In case 1, deviation at the rotor exit causes the rotor exit velocity to change from the solid arrow (no deviation) to the arrow with the dotted line. In case 2, the boundary layer blockage causes the change from an ideal situation with no blockage.

$$\frac{\rho u_{x,2} u_{y,2} W_2}{\rho u_{x,1} u_{y,1} W_1} = \frac{u_{y,2}}{u_{y,1}} = \frac{|u_2| \sin \beta_2}{|u_1| \sin \beta_1} \tag{A1}$$

The circumferential blade force per unit flow area normalized by the inlet flux of circumferential momentum per unit flow area is thus

$$\frac{F_\theta}{\rho u_{x,1} u_{y,1}} = 1 - \frac{|u_2| \sin \beta_2}{|u_1| \sin \beta_1} \tag{A2}$$

From Bernoulli's equation, we can write $|u_2|/|u_1|$ in terms of the static pressure rise coefficient. Combining this with Eq. (A2) yields

$$\frac{F_\theta}{\rho u_{x,1} u_{y,1}} = 1 - (1 - C_p)^{0.5} \frac{\sin \beta_2}{\sin \beta_1} \tag{A3}$$

For case 1, an increase in the deviation angle increases β_2 and decreases C_p, both of which, as in Eq. (A3), decrease the circumferential force component. For case 2, an increase in blockage with negligible deviation, there is an effect on C_p only, but again, a decrease in the circumferential blade force.

Using the scaling for relative stagnation pressure nonuniformity from the compressor simulations, the results of Wolf and Johnston can be used to estimate the variation in the static pressure rise coefficient that would accompany a phase change in the relative stagnation pressure profile at the inlet, and hence, a change in the circumferential force. The ratio of cos β_2 to cos β_1 yields the area ratio appropriate for the compressor geometry. For case 1 (deviation) the change in the circumferential force due to change in the position of the inlet profile is estimated to be 5.6%. For case 2 (blockage), the estimated variation is 3.0%. In the numerical simulations, there is a combination of flow deviation and blockage, but the latter is dominant, so one could expect the variation to fall within the range of 3–6%. In accord with these estimates, the MISES calculations carried out (described in Sec. 4.1) show roughly 4% variation in the circumferential blade force, depending on the position of the inlet profile.

References

[1] Gorrell, S., Okiishi, T., and Copenhaver, W., 2003, "Stator-Rotor Interactions in a Transonic Compressor: Part 1—Effect of Blade-Row Spacing on Performance," ASME J. Turbomach., **125**, pp. 328–335.

[2] Gorrell, S., Car, D., Puterbaugh, S., Estevadeordal, J., and Okiishi, T., 2006, "An Investigation of Wake-Shock Interactions in a Transonic Compressor With DPIV and Time-Accurate CFD," ASME J. Turbomach., **128**, pp. 616–626.

[3] Smith, L., 1970, "Casing Boundary Layers in Multistage Axial Flow Compressors," *Flow Research on Blading*, Elsevier Publishing Company, Amsterdam, Netherlands.

[4] Hetherington, R., and Moritz, R. R., 1975, "The Influence of Unsteady Flow Phenomena on the Design and Operation of Aero Engines," *Proceedings of the AGARD Conference on Unsteady Phenomena in Turbomachines*, North Atlantic Treaty Organization, AGARD Paper No. CP-177.

[5] Mikolajczak, A. A., 1975, "The Practical Importance of Unsteady Flow," *Proceedings of the AGARD Conference on Unsteady Phenomena in Turbomachines*, AGARD Paper No. CP-177.

[6] Smith, L., 1966, "Wake Dispersion in Turbomachines," ASME J. Basic Eng., **88**, pp. 688–690.

[7] Greitzer, E., Tan, C., and Graf, M., 2004, *Internal Flow: Concepts and Applications*, Cambridge University Press, Cambridge, UK.

[8] Valkov, T., and Tan, C., 1999, "Effects of Upstream Rotor Vortical Disturbances on Time-Average Performance of Axial Compressor Stator: Part 1—Framework of Technical Approach and Rotor Wakes-Stator Blade Interaction Interaction," ASME J. Turbomach., **121**(3), pp. 377–386.

[9] Valkov, T., and Tan, C., 1999, "Effects of Upstream Rotor Vortical Disturbances on Time-Average Performance of Axial Compressor Stator: Part 2—Rotor Tip Leakage and Discrete Streamwise Vortex-Stator Blade Interaction," ASME J. Turbomach., **121**(3), pp. 387–397.

[10] Adamczyk, J. J., 1996, "Wake Mixing in Axial Flow Compressors," ASME Paper No. 96-GT-29.

[11] Zachcial, A. and Nuernberger, D., 2003, "A Numerical Study on the Influence of Vane-Blade Spacing on a Compressor Stage and Sub- and Transonic Operating Conditions," ASME Paper No. GT2003-38020.

[12] Botros, B., 2008, "Impact of Unsteady Flow Processes on the Performance of a High Speed Axial Flow Compressor," MS thesis, Department of Mechanical Engineering, Massachusetts Institute of Technology, Cambridge, MA.

[13] Chen, J., 2001, "A Parallel Flow Solver for Unsteady Multiple Blade Row Turbomachinery Simulations," ASME Paper No. GT2001-0348.

[14] Van Zante, D., Chen, J., Hathaway, M., and Chriss, R., 2008, "The Influence of Compressor Blade Row Interaction Modeling on Performance Estimates From Time-Accurate, Multistage, Navier–Stokes Simulations," ASME J. Turbomach., **130**, p. 011009.
[15] Gorrell, S., Car, D., Puterbaugh, S., Estevadeordal, J., and Okiishi, T., 2005, "An Investigation of Wake-Shock Interactions in a Transonic Compressor With DPIV and Time-Accurate CFD," ASME Paper No. GT2005-69107.
[16] Wolf, S., and Johnston, J., 1966, "Effects of Nonuniform Inlet Velocity Profiles on Flow Regimes and Performance in Two-Dimensional Diffusers," Thermosciences Division, Stanford University, Stanford, CA, Technical Report No. PD-12.
[17] Wolf, S., and Johnston, J., 1969, "Effects of Nonuniform Inlet Velocity Profiles on Flow Regimes and Performance in Two-Dimensional Diffusers," ASME J. Basic Eng., **91**, pp. 462–474.
[18] Key, N., Lawless, P., and Fleeter, S., 2008, "An Investigation of the Flow Physics of Vane Clocking Using Unsteady Flow Measurements," ASME Paper No. GT2008-51091.
[19] Drela, M., and Youngren, H., 1998, "A User's Guide to MISES 2.53," MIT Fluid Dynamics Research Laboratory.
[20] Schreiber, H., and Starken, H., 1984, "Experimental Investigation of a Transonic Compressor Rotor Blade Section," ASME J. Eng. Gas Turbines Power, **106**, pp. 288–294.
[21] List, M., Gorrell, S., and Turner, M., 2008, "Investigation of Loss Generation in an Embedded Transonic Fan Stage at Several Gaps Using High Fidelity, Time-Accurate CFD," ASME Paper No. GT2008-51220.
[22] Khalid, S., Khalsa, A., Waitz, I., Tan, C., Greitzer, E., Cumpsty, N., Adamczyk, J., and Marble, F., 1999, "Endwall Blockage in Axial Compressors," ASME J. Turbomach., **121**, pp. 499–509.